IEEE Access
Multidisciplinary | Rapid Review | Open Access Journal

Received February 11, 2020, accepted March 26, 2020, date of publication March 30, 2020, date of current version April 15, 2020.

Digital Object Identifier 10.1109/ACCESS.2020.2984282

Vibration Measurement Based on the Local Maximum Detection Algorithm for Laser Self-Mixing Interferometry

ZIHUA ZHANG[1], CHUNLEI JIANG[2], LIQUN SHEN[1], CHENGWEI LI[1], AND ZHEN HUANG[3]

[1]School of Instrumentation Science and Engineering, Harbin Institute of Technology, Harbin 150001, China
[2]College of Electrical and Information Engineering, Northeast Petroleum University, Daqing 163318, China
[3]School of Physics Science and Technology, Lingnan Normal University, Zhanjiang 524048, China

Corresponding authors: Zihua Zhang (zhanghua_0813@126.com) and Chengwei Li (lcw@hit.edu.cn)

This work was supported in part by the National Natural Science Foundation of China under Grant 61705095, and in part by the Science and Technology Planning Project of Guangdong Province under Grant 2017A010102022.

ABSTRACT A novel laser self-mixing interferometry vibration measurement algorithm based on the local maximum detection technique is proposed, that can reconstruct micro vibrations rapidly and easily. In this article, the principles of the local maximum detection algorithm are analyzed in detail, and the process of solving the window function is emphasized. The major advantage of the method is that it does not involve any complicated calculations and removes the need for optical/electromechanical components. The validity of the presented method is confirmed by means of simulated signals and demonstrated via several experiments for harmonic and aleatory motion.

INDEX TERMS Vibration measurement, local maximum detection, self-mixing interferometry.

I. INTRODUCTION

Laser self-mixing interferometry (SMI), which is also called the laser optical feedback interference effect, is an emerging and promising nondestructive optical measurement technique [1], [2]. This method reduces the complexity of the optical system configuration compared with that under traditional double-beam interferometry [3]–[6]. SMI occurs when a portion of a laser diode (LD) output beam is reflected or diffused by a moving target and returned to the laser cavity. The reinjected laser beam carries the moving target information and mixes with the internal light, causing variations in the wavelength of the laser and the optical output power. The output SMI power is detected by a built-in monitor photodiode (PD). The SMI technique is used in several fields of research in applications such as measuring absolute distance [7], [8]; displacement [9]; vibration [10], [11]; and velocity [12], [13]; and imaging [14]; and laser parameter measurement [15], [16] due to its compactness, self-alignment, and low cost.

An SMI signal has a $\lambda/2$ fringe resolution, and the accuracy depends on the wavelength changes [1]. To increase the measurement accuracy beyond a half- wavelength, Jiang *et al.* proposed an improved transition detection algorithm that can differentiate between different SMI feedback levels [9]. However, false transitions could lead to measurement error. Arriaga *et al.* proposed a fringe detection method that is based on the Hilbert transform, and the algorithm shows immunity to speckle signal interference in reconstructing displacement [17]; however, the phase unwrapping process is slightly complicated. Bes *et al.* proposed a phase unwrapping method (PUM) that can estimate the optical feedback level factor C and line-width enhancement factor α, and this method can achieve a resolution of $\lambda/16$ [18]. However, PUM can adapt to the moderate feedback regime only. Huang *et al.* proposed a dominant harmonic order determination method to reconstruct external target vibration [19]; however, it can measure sinusoidal vibration only. Wang *et al.* proposed an integral reconstruction method for displacement measurements, and the relative error was less than 3.2% [20]. However, this method can be used under the very weak feedback regime only. Zhang *et al.* proposed a new demodulation algorithm based on multiple Hilbert transforms (MHT) for SMI [11]. However, this method has a large relative error.

The associate editor coordinating the review of this manuscript and approving it for publication was Jenny Mahoney.

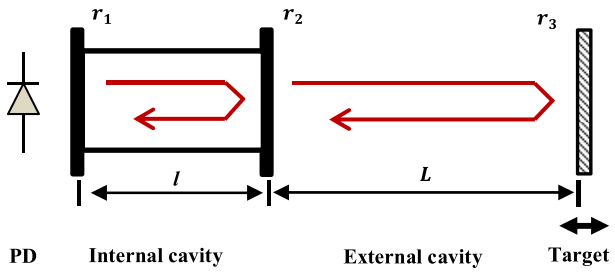

FIGURE 1. Schematic diagram of two Fabry–Pérot cavities, depicting self-mixing interference.

An effective micro vibration measurement algorithm based on local maximum detection (LMD) for self-mixing signals is therefore proposed in this work. First, the local maximum points (LMPs) of the SMI signal are obtained to determine the unwrapped laser external phase $\phi_F(t)$. However, the obtained LMPs do not contain directivity. Second, a window function that is based on adopting the median of the derivative of the SMI signal is proposed to determine the correct direction of the LMPs. Third, we use the cubic spline interpolation method to fit the micro vibration curve. While maintaining the inherent simplicity, compactness and low cost of the measurement system, the target vibration can be easily reconstructed.

The rest of this study is organized as follows. First, the theory of SMI phenomenon is derived by two Fabry–Pérot cavities. Second, the proposed LMD algorithm is analyzed in detail, and the process of the window function is emphasized. Finally, the algorithm is validated through numerical simulations and experiments.

II. LASER SELF-MIXING INTERFERENCE EFFECT

Laser self-mixing interference theory was first presented by Lang and Kobayashi in 1980 [21]; the well-known equation is also named after them. Many researchers have studied *Lang–Kobayashi* theory [1], [2], [22]. The vibration of the external target induces the modulation of the length of the external cavity, which leads to SMI. The basic theories of the self-mixing interference effect can be explained by two Fabry–Pérot cavities, as shown in Fig. 1 [22], in which r_1 and r_2 denote the amplitude reflectivity of LD facets, r_3 is the amplitude reflectivity of the external target, l is the length of the laser cavity and L represents the length of the external cavity. The output power signal is detected by a PD.

According to *Lang–Kobayashi* theory, the relationship between the external phase $\phi_F(t)$ and the laser output power P_F of the self-mixing interference is expressed as

$$P_F(t) = P_0[1 + m\cos(\phi_F(t))], \tag{1}$$

where P_0 refers to the laser output power under free beam running conditions. m represents the modulation index of SMI and is affected by the reflection coefficient of the target surface [23]. In (1), the external phase $\phi_F(t)$ can be derived as

$$\cos(\phi_F(t)) = (P_F/P_0 - 1)/m. \tag{2}$$

When the laser self-mixing effect occurs, the external round trip phase should satisfy

$$\phi_0(t) = \phi_F(t) + C\sin[\phi_F(t) + \arctan(\alpha)], \tag{3}$$

where $\phi_0(t)$ represents the external phase without optical feedback, α refers to the line-width enhancement factor, and C denotes the feedback level parameter. According to [24], $0 < C \leq 1$ is a weak feedback regime, $1 < C \leq 4.6$ is a moderate feedback regime and $C > 4.6$ is a strong feedback regime. For $C > 4.6$, the SMI fringes become sawtooth-like and exhibit hysteresis. For the moderate feedback regime, the piecewise transition detection algorithm was proposed on the basis of SMI signal differentials [9], [18], [25]. However, identifying the direction of the target directly from the SMI signal in the weak feedback regime is difficult because the signals are nearly sinusoidal. Therefore, in this study, only weak optical feedback levels are discussed.

The laser external phase without and with optical feedback can be expressed as

$$\phi_0(t) = 2\pi \times 2L(t)/\lambda_0, \tag{4}$$

$$\phi_F(t) = 2\pi \times 2L(t)/\lambda_F, \tag{5}$$

where λ_0 represents the initial wavelength of the laser and λ_F represents the wavelength with optical feedback. Moreover, given the weak feedback regime [9] $\phi_0(t) \approx \phi_F(t)$, and according to (3), the external target vibration expression can be written as

$$L(t) = \frac{\lambda_0}{2 \times 2\pi}\phi_F(t). \tag{6}$$

III. ALGORITHM DESCRIPTION

A. PRINCIPLE OF LMD

This study presents a new algorithm that is based on the LMD technique to unwrap the correct external phase $\phi_F(t)$ and reconstruct micro vibrations. Figure 2 shows the simulation of a self-mixing interference signal; the simulation program comes from reference [26]. The self-mixing interference signal generated in Fig. 2(a) comes from equation (1) and represents the output power of the laser. In Fig. 2(a), the numerical simulation is operated under $C = 0.1$, and the line-width enhancement factor $\alpha = 4.6$. The simulated wavelength of the LD is 650 nm, and the original external cavity length between the LD and the target is $L_0 = 0.1\,m$. The harmonic vibration is driven at a frequency of 100 Hz and an amplitude of 1.8 μm. The sampling frequency is 200 kHz, and 4000 sampling points exist. The local maximum points (LMPs) of the SMI signal are shown in Fig. 2(b).

The LMPs of the SMI are acquired. However, the detection of LMPs does not contain directivity [22]. We propose the window function method based on the inverse point to obtain the right direction for the LMPs.

The correct window function is based on adopting the median of the derivative of the SMI signal [20], [22]. Fig. 3(a)

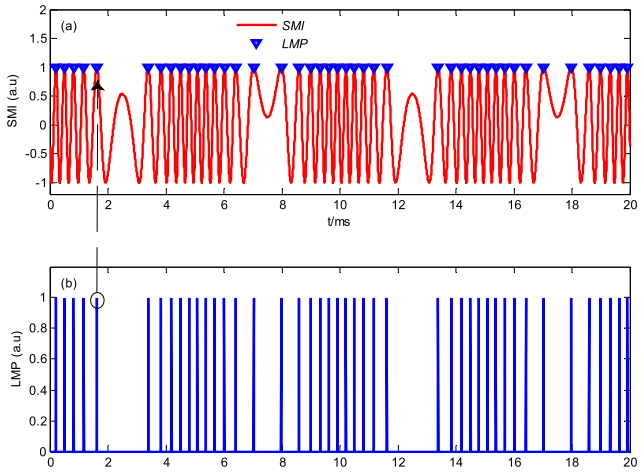

FIGURE 2. Local maximum points of the self-mixing signal. (a) SMI simulation with C = 0.1. (b) The local maximum points.

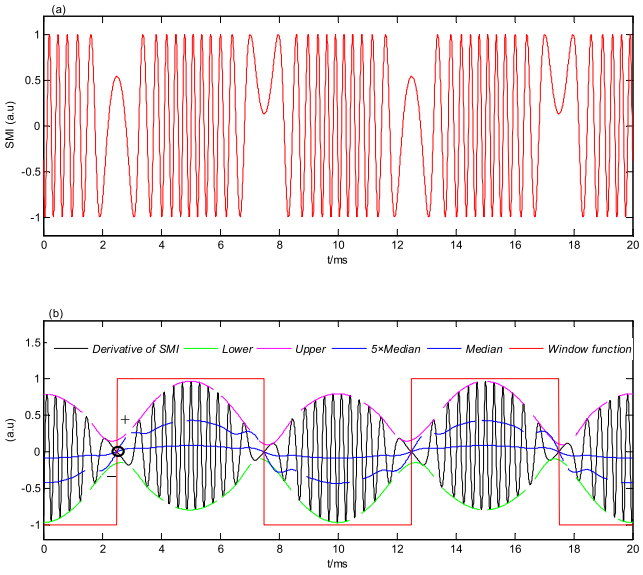

FIGURE 3. Window function of the self-mixing signal. (a) SMI with C = 0.1. (b) Derivative of the SMI signal (black solid curve), its lower and upper envelopes (green and magenta dashed curves, respectively) and the median of the derivative signal (blue solid curve) compared with its magnified (five times) version (blue dashed curve) and the window function of the SMI (red solid curve).

shows the simulated SMI signal for $C = 0.1$. As presented in Fig. 3(b), the black solid curve represents the derivative signal of SMI, with its lower and upper envelopes represented by green and magenta dashed lines, respectively. The upper and lower envelopes are expressed as $env_{\max}(t)$ and $env_{\min}(t)$, respectively. Moreover, the median of the derivative signal can be derived by

$$med(t) = env_{\max}(t) - [env_{\max}(t) - env_{\min}(t)]/2, \quad (7)$$

which is shown in Fig. 3(b) by the blue solid curve, from which we can see that the signs of $med(t)$ indicate the correct directivity for the moving target. The median curve is magnified five times, as presented by the blue dashed curve,

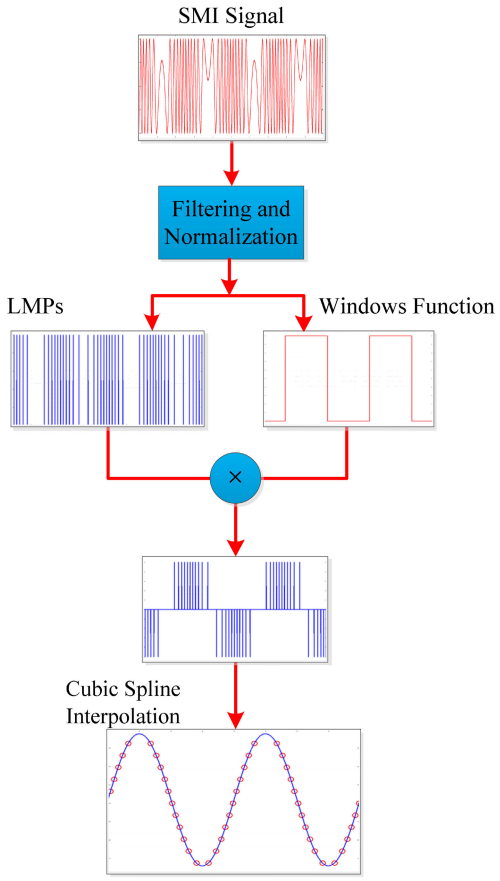

FIGURE 4. Block diagram of the LMD algorithm.

to facilitate comparison of this curve with the other curves in a single graph. The window function is thus obtained in accordance with the inverse point (between + and −).

A block diagram of the proposed algorithm is shown in Fig. 4. First, the SMI signal is filtered and normalized. Then, the LMPs of the SMI signal are obtained. Moreover, we can obtain the window function by adopting the median of the derivative of the SMI. Next, we can obtain the modified LMPs that contain the correct directivity by using the LMPs to multiply the window function. After the LMPs of the SMI signal are correctly detected, the micro-vibration can be reconstructed by the fringe counting method providing $\lambda/2$ resolution, and other reconstruction methods. In this study, the cubic spline interpolation method [27] is used to reconstruct the micro vibrations, as shown in the block diagram.

B. NUMERICAL SIMULATION

The vibration reconstruction based on the proposed method is tested with MATLAB software.

The values of the parameters and variables in the numerical simulation are listed in Table 1.

The sampling frequency is 200 kHz, and 8000 sampling points exist. The red curve in Fig. 5(a) presents the simulated SMI signal. The blue points in Fig. 5(b) are the LMPs with

TABLE 1. Values of the variables in simulation.

Variables	Definition	Values
C	Optical feedback parameter	0.1
α	Line-width enhancement factor	4.6
λ_0	Laser initial wavelength	650 nm
L_0	Original external cavity length between the LD and the target	0.1 m

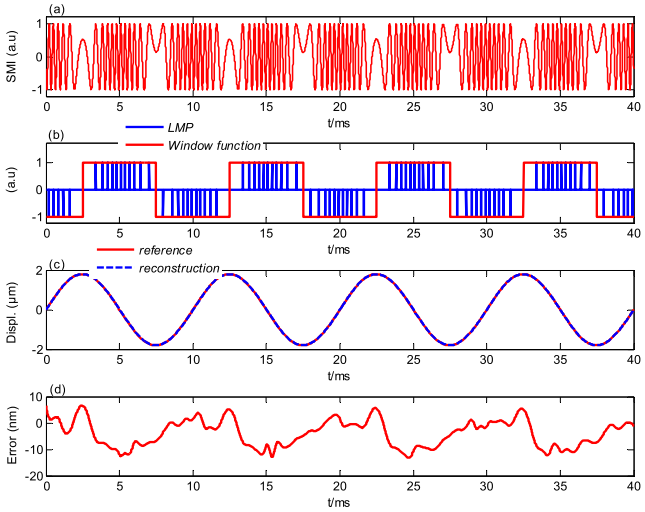

FIGURE 5. Simulation of harmonic vibration with C = 0.1. (a) SMI signal. (b) Local maximum points (blue) and window function (red). (c) Reference and reconstruction vibration (red solid and blue dashed lines, respectively). (d) Absolute error.

the correct direction, and the red curve is the window function of the SMI signal. In Fig. 5(c), the harmonic vibration is driven at a frequency of 100 Hz and amplitude of 1.8 μm as a reference (in red), and the blue dashed line presents the reconstruction vibration. Figure 5(d) illustrates the absolute error between the reference and vibration reconstruction, from which the maximum absolute error is -13.2 nm.

The vibration reconstruction is performed using a simulated aleatory movement to confirm the generality of the proposed LMD algorithm. The aleatory movement is organized using a sinusoidal wave of 100 Hz modulated by a 50 Hz sinusoidal wave with a modulation depth of 50%. A total of 8000 sampling points exist. The SMI signal of the aleatory motion is shown in Fig. 6(a), which indicates that the number of SMI fringes varies with the amount of displacement on both sides of the inverse points. As illustrated in Fig. 6(b), the black solid curve represents the derivative signal of the SMI, and its lower and upper envelopes are represented by the green and magenta dashed lines, respectively. The median of the derivative signal is presented by the blue dashed curve,

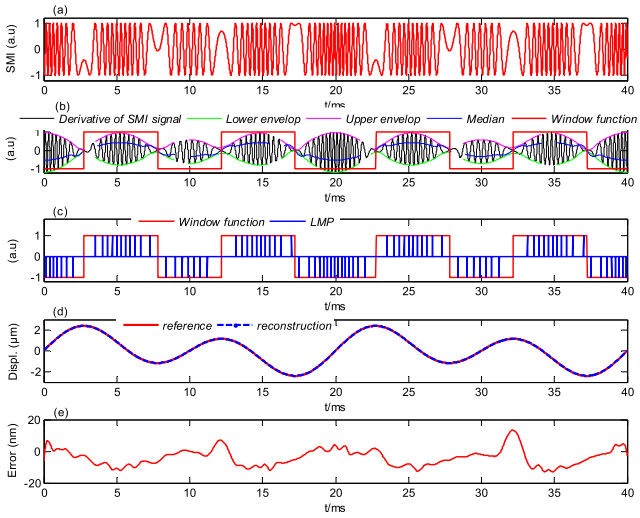

FIGURE 6. Simulation of aleatory vibration with C = 0.1. (a) SMI signal. (b) Derivative of the SMI signal (black), its lower and upper envelopes (green and magenta dashed curves, respectively), the median of the derivative signal magnified five times (blue dashed curve) and the window function (red). (c) Local maximum points (blue) and window function (red). (d) Reference and reconstruction vibration (red solid and blue dashed curves, respectively). (e) Absolute error.

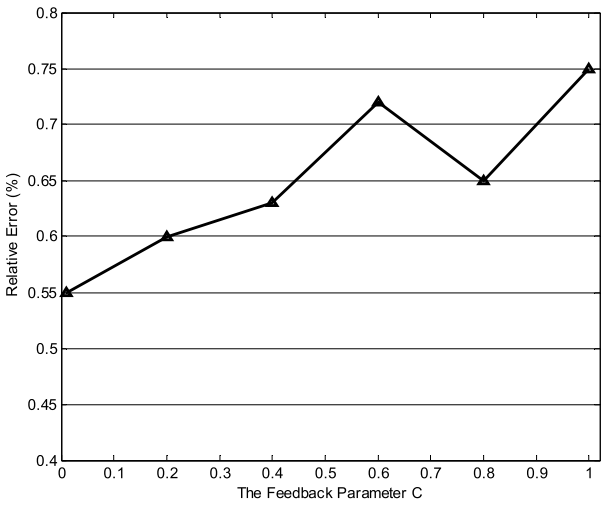

FIGURE 7. Simulation of target vibration with different C values under a weak optical feedback regime.

which is magnified five times for clarity. The blue points in Fig. 6(c) are the correct LMPs, and the red curve is the window function. In Fig. 6(d), the aleatory vibration is driven with a peak-to-peak amplitude of 3.5 μm as the reference (in red), and the blue dashed curve presents the reconstruction vibration. Figure 6(e) represents the absolute error between the reference and vibration reconstruction, from which the maximum absolute error is 13.34 nm.

Furthermore, the influence of the optical feedback level on the vibration measurement is considered. The simulation results with different C values under the weak feedback regime are shown in Fig. 7. The remaining parameters in the simulation series are consistent with those in Fig. 5. Figure 7 indicates that the minimum relative error is 0.55%

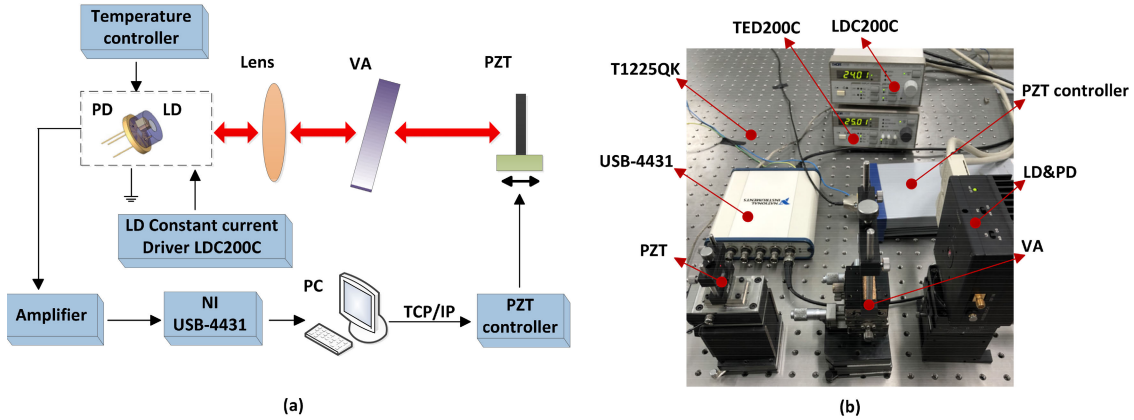

FIGURE 8. Experimental system (a) Schematic diagram. (b) Experimental setup.

when $C = 0.01$, with a peak-to-peak error of 19.98 nm and a peak-to-peak vibration amplitude of 3.6 μm. The maximum relative error is 0.75% when $C = 1.0$, with an absolute peak-to-peak error is 26.99 nm. The simulation results in Fig. 7 show that the proposed LMD algorithm has high precision, with all the relative errors being less than 1% under the weak feedback regime. The findings also verify that the algorithm is only slightly influenced by the optical feedback level under the weak feedback regime.

IV. EXPERIMENTAL VALIDATIONS

Experiments are performed to verify the effectiveness of the proposed LMD algorithm. Figure 8 shows the experimental photos. A low-cost commercial InGaAIP laser diode (LD, QL65D5SA, QSI) is used as a light source to generate the SMI effect. When the LD is driven by a constant current driver (LDC200C, Thorlabs) of 24 mA, it generates a single longitudinal mode beam with a wavelength of 650 nm, and the typical light output power is 5 mW. According to the specification of the laser diode constant current driver LDC200C, the typical value of the output current drift is less than 1 μA under continuous operation for 24 hours. The constant current driver performs well against temperature drift. A variable attenuator (VA) is used to adjust the amount of optical feedback into the inner laser cavity. A mirror is fixed on a piezoelectric transducer (PZT, P753.1CD, PI) as a standard vibrating target with a traveling distance of 12 μm. The resolution of 0.05 nm under closed loop control makes PZT a high-precision reference in vibration measurement experiments. The current variation of the laser diode is monitored by a photodiode (PD) packaged in the LD. The current is then converted into voltage and sent through by a trans-conductance amplifier. Subsequently, the voltage signal is digitized with a data acquisition module (USB-4431, NI) and finally processed on a computer.

Temperature is an important parameter in self-mixing interference tests. In the experiments, a temperature controller (TED200C, Thorlabs) is used to maintain a constant temperature for the laser diode, and to avoid the influence of temperature changes on the experimental results. Moreover, the experimental equipment is placed on a precision optical table (T1225QK, Thorlabs) for the experiments to avoid the effects of mechanical vibration. All these measures can guarantee the stability of the system over time.

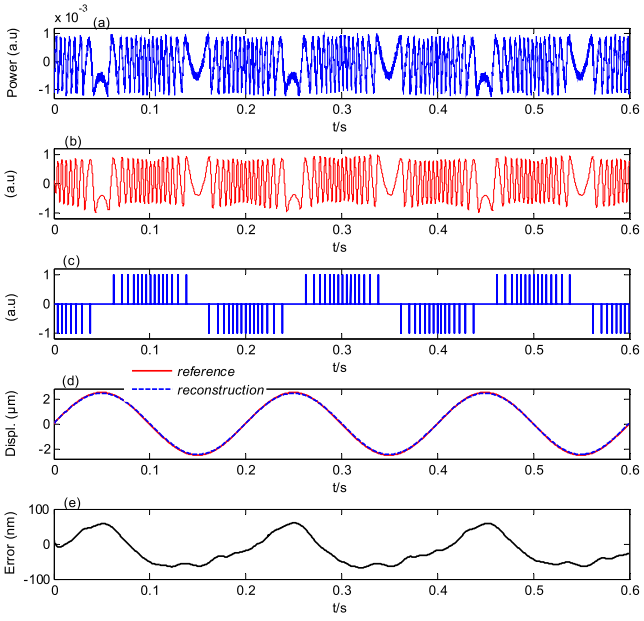

FIGURE 9. Harmonic vibration reconstruction experiments with C = 0.1. (a) Experimental SMI signal. (b) Filtered and normalized signal. (c) Local maximum points. (d) Reference and reconstruction vibration (red solid and blue dashed curves, respectively). (e) Absolute error.

The experiments are conducted in the weak feedback regime, as shown in Fig. 9. The harmonic vibration of the PZT is controlled at a frequency of 5 Hz and a peak-to-peak amplitude of 5 μm. The sampling frequency is 50 kHz, and 30000 sampling points are used. In the experiment, a 300 Hz low-pass filter is used to filter the PD output acquisition signal, and the filtering signal is normalized. The curve in Fig. 9(a) shows the experimental SMI signal for $C = 0.1$. The filtered and normalized signal is shown in Fig. 9(b). Figure 9(c) presents the LMPs of the SMI with the

correct direction. The blue dashed curve in Fig. 9(d) presents the reconstruction measurement through the LMD reconstruction algorithm, and the red solid curve provides a reference for the PZT vibration. Figure 9(e) shows the absolute error between the reference and the reconstruction, with a maximum absolute error of 67.9 nm and a peak-to-peak relative error of 2.6%.

To further illustrate the reliability of the proposed method, we perform several experiments with $C = 0.1$. The PZT vibrates at a frequency of 5 Hz and peak-to-peak amplitudes from 2.0 μm to 10.0 μm, with a step size of 1.0 μm. Each experiment is repeated 10 times, and the sampling frequency is 50 kHz. The analysis results are shown in Fig. 10, in which the red circles represent the mean relative error and the black error bars correspond to the standard error of the reconstruction vibration under weak feedback.

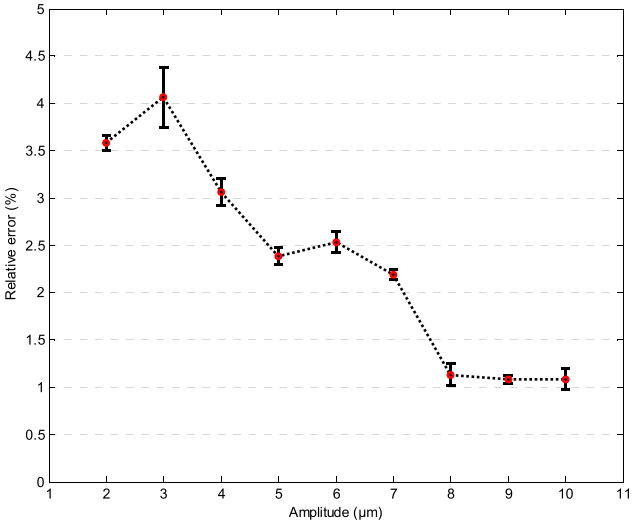

FIGURE 10. Relative error of different amplitude vibrations.

Figure 10 indicates that the relative errors of all the vibration reconstruction experiments are less than 5%. Moreover, the relative error of reconstruction tends to decrease gradually with increasing vibration amplitude.

The accuracy of MHT [11] and the proposed method are compared to show the performance of the LMD algorithm. The reconstruction peak-to-peak absolute error of the two methods at different amplitudes is shown in Table 2. The harmonic vibration is controlled at a frequency of 5 Hz, peak-to-peak amplitudes from 2 μm to 7 μm and a constant sampling frequency of 50 kHz. Both of the optical feedback levels of the reconstructed SMI signal are estimated at 0.1. The table shows that all the reconstruction errors of the micro vibration except that at 3 μm are better than those of MHT.

Next, the target is driven to move in a triangular waveform with a frequency of 5 Hz and peak-to-peak amplitude of 4.6 μm. The number of sampling points is 30000, and the sampling frequency is 50 kHz. The reconstruction process is shown in Fig. 11. The power signal of the SMI is presented in Fig. 11(a). Figure 11(b) shows the processed SMI signal,

TABLE 2. Comparison of errors between MHT and LMD.

Vibration amplitude (μm)	Error of MHT [a] (nm)	Error of LMD (nm)
2	118.0	71.6
3	113.0	122.0
4	146.6	122.6
5	166.7	119.4
6	228.0	151.8
7	200.7	153.1

[a]The data are from reference [11] and are the average of three repeated trials.

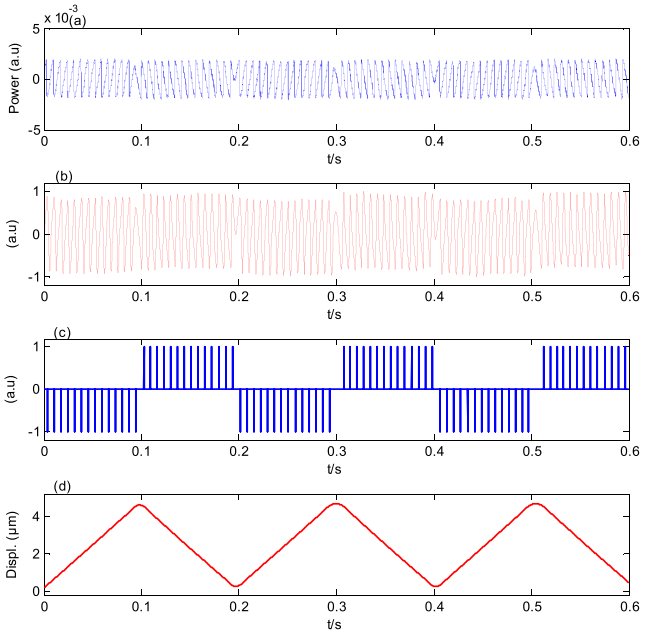

FIGURE 11. Triangular waveform vibration reconstruction experiments with C = 0.1. (a) Experimental SMI signal. (b) Filtered and normalized signal. (c) Local maximum points. (d) Reconstruction vibration.

whereas Fig. 11(c) illustrates the local maximum points of the SMI with the correct direction. The corresponding peak-to-peak amplitude of the reconstructed waveform is 4.539 μm for a maximum vibration amplitude of 4.6 μm, which is shown in Fig. 11(d).

Furthermore, we conduct a group of aleatory vibration reconstruction experiments to verify the generality of the proposed algorithm, as shown in Fig. 12. The target vibration is a sine wave of 10 Hz modulated by a 5 Hz sine wave with a modulation depth of 50%, as shown in Fig. 12(d) by the red solid curve. The blue dashed curve presents the reconstruction vibration through the LMD reconstruction algorithm. The number of sampling points is 30000, and the other parameters are the same as those in Fig. 9. The curve in Fig. 12(a) shows the experimental SMI signal under weak feedback for $C = 0.1$, and the filtered and normalized signal is shown in Fig. 12(b). Figure 12(c) presents the local maximum points

TABLE 3. Comparison of computing times of the PUM, integral, MHT and LMD methods at different sampling rates.

Sampling rates (kHz)	Time of PUM (s)	Time of integral method (s)	Time of MHT (s)	Time of LMD method (s)
20	0.271	0.139	0.206	0.056
40	0.283	0.144	0.211	0.057
60	0.362	0.156	0.218	0.057
80	0.398	0.159	0.223	0.060
100	0.451	0.175	0.230	0.061

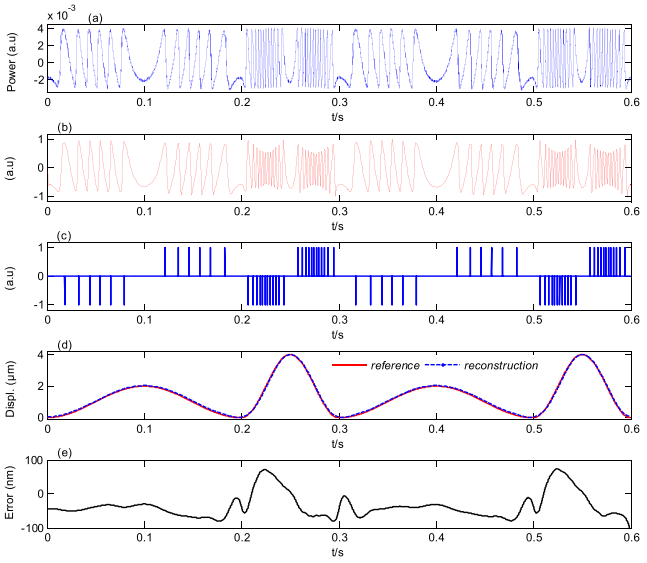

FIGURE 12. Aleatory vibration reconstruction experiments with C = 0.1. (a) Experimental SMI signal. (b) Filtered and normalized SMI signal. (c) Local maximum points. (d) Reference and reconstruction vibration (red solid and blue dashed curves, respectively). (e) Absolute error.

of the SMI. The corresponding peak-to-peak amplitude of the reconstructed waveform is 3.977 μm for a maximum vibration amplitude of 2.0 μm. Figure 12(e) shows the absolute error between the reference and reconstruction, with a peak-to-peak relative error of 4.85%.

Finally, several groups of experiments are conducted at different sampling rates (from 20 kHz to 100 kHz) with an interval of 20 kHz to compare the computing times of the proposed LMD method, the MHT method [11], the integral reconstruction method [20] and the PUM method [18]. For comparison, the harmonic vibration experimental parameters are set as follows: 2 μm peak-to-peak amplitude and 5 Hz frequency. The SMI signal of one period is reconstructed. The computing times of the four reconstruction methods, which are listed in Table 3, are calculated using MATLAB. The computing times of all the methods increase gradually as the sampling frequency increases, but the LMD method has a shorter computing time than the other three methods. This finding is expected, given that the proposed LMD algorithm does not require any integrals, Hilbert transformations or phase unwrapping operations. Therefore, it has a faster calculation speed than the compared methods.

It should also be noted that the measurement results are also correlated with the light intensity disturbance [28]. Automatic gain control can be used to stabilize the signal to minimize the impact on the measurement; however, the influence of the light intensity disturbance remains difficult to eliminate thoroughly [29]. Therefore, we will minimize the influence of the intensity distribution on the measurement results in the near future.

V. CONCLUSION

In this study, a simple and effective reconstruction method for vibration is proposed. With a combination of local maximum detection and the window function technique, micro vibrations can be reconstructed under the weak feedback regime in self-mixing interference. The repeated experimental results show that the relative error is less than 5%. The optical path is simple and does not involve any complicated calculations; thus, this method can be applied in semiconductor laser self-mixing vibration measurements. Therefore, the proposed method provides a beneficial exploration of micro vibration measurements.

CONFLICT OF INTERESTS

The authors declare that there is no conflict of interests regarding the publication of this paper.

REFERENCES

[1] T. Taimre, M. Nikolić, K. Bertling, Y. L. Lim, T. Bosch, and A. D. Rakić, "Laser feedback interferometry: A tutorial on the self-mixing effect for coherent sensing," *Adv. Opt. Photon.*, vol. 7, no. 3, pp. 570–631, Sep. 2015.
[2] S. Donati, "Developing self-mixing interferometry for instrumentation and measurements," *Laser Photon. Rev.*, vol. 6, no. 3, pp. 393–417, May 2012.
[3] P. Chen, Y. Liu, B. Gao, and C. Jiang, "Modeling and experimental verification of laser self-mixing interference phenomenon with the structure of two-external-cavity feedback," *Opt. Commun.*, vol. 410, pp. 690–693, Mar. 2018.
[4] Y. Tao, W. Xia, M. Wang, D. Guo, and H. Hao, "Integration of polarization-multiplexing and phase-shifting in nanometric two dimensional self-mixing measurement," *Opt. Express*, vol. 25, no. 3, pp. 2285–2298, Feb. 2017.
[5] L. Lu, J. Yang, L. Zhai, R. Wang, Z. Cao, and B. Yu, "Self-mixing interference measurement system of a fiber ring laser with ultra-narrow linewidth," *Opt. Express*, vol. 20, no. 8, pp. 8598–8607, Apr. 2012.
[6] K. Kou, X. Li, L. Li, H. Li, and T. Wu, "Absolute distance estimation with improved genetic algorithm in laser self-mixing scheme," *Opt. Laser Technol.*, vol. 68, pp. 113–119, May 2015.
[7] Z. Duan, Y. Yu, B. Gao, and C. Jiang, "Absolute distance measurement based on multiple self-mixing interferometry," *Opt. Commun.*, vol. 389, pp. 270–274, Apr. 2017.

[8] D. Guo and M. Wang, "Self-mixing interferometry based on a double-modulation technique for absolute distance measurement," *Appl. Opt.*, vol. 46, no. 9, pp. 1486–1491, Mar. 2007.

[9] C. Jiang, C. Li, and Y. Wang, "Improved transition detection algorithm for a self-mixing displacement sensor," *Optik*, vol. 127, no. 14, pp. 5603–5612, Jul. 2016.

[10] V. Girardeau, O. Jacquin, O. Hugon, and E. Lacot, "Ultrasound vibration measurements based on laser optical feedback imaging," *Appl. Opt.*, vol. 57, no. 26, pp. 7634–7643, Sep. 2018.

[11] Z. Zhang, C. Li, and Z. Huang, "Vibration measurement based on multiple Hilbert transform for self-mixing interferometry," *Opt. Commun.*, vol. 436, pp. 192–196, Apr. 2019.

[12] B. Gao, C. Qing, S. Yin, C. Peng, and C. Jiang, "Measurement of rotation speed based on double-beam self-mixing speckle interference," *Opt. Lett.*, vol. 43, no. 7, pp. 1531–1533, Apr. 2018.

[13] Z. Du, L. Lu, W. Zhang, B. Yang, H. Gui, and B. Yu, "Measurement of the velocity inside an all-fiber DBR laser by self-mixing technique," *Appl. Phys. B*, vol. 113, no. 1, pp. 153–158, Oct. 2013.

[14] O. Jacquin, W. Glastre, E. Lacot, O. Hugon, H. Guillet de Chatellus, and F. Ramaz, "Acousto-optic laser optical feedback imaging," *Opt. Lett.*, vol. 37, no. 13, pp. 2514–2516, Jul. 2012.

[15] Y. Zhao, G. Xu, C. Zhang, K. Liu, and L. Lu, "Vibration displacement immunization model for measuring the free spectral range by means of a laser self-mixing velocimeter," *Appl. Opt.*, vol. 58, no. 20, pp. 5540–5546, Jul. 2019.

[16] Y. Fan, Y. Yu, J. Xi, and Q. Guo, "Dynamic stability analysis for a self-mixing interferometry system," *Opt. Express*, vol. 22, no. 23, pp. 29260–29269, Nov. 2014.

[17] A. L. Arriaga, F. Bony, and T. Bosch, "Speckle-insensitive fringe detection method based on Hilbert transform for self-mixing interferometry," *Appl. Opt.*, vol. 53, no. 30, pp. 6954–6962, Oct. 2014.

[18] C. Bes, G. Plantier, and T. Bosch, "Displacement measurements using a self-mixing laser diode under moderate feedback," *IEEE Trans. Instrum. Meas.*, vol. 55, no. 4, pp. 1101–1105, Aug. 2006.

[19] Z. Huang, X. Sun, and C. Li, "Self-mixing interference signal analysis based on Fourier transform method for vibration measurement," *Opt. Eng.*, vol. 52, no. 5, May 2013, Art. no. 053601.

[20] X. Wang, Y. Yuan, S. Luqing, B. Gao, and P. Chen, "Self-mixing interference displacement measurement under very weak feedback regime based on integral reconstruction method," *Opt. Commun.*, vol. 445, pp. 236–240, Aug. 2019.

[21] R. Lang and K. Kobayashi, "External optical feedback effects on semiconductor injection laser properties," *IEEE J. Quantum Electron.*, vol. 16, no. 3, pp. 347–355, Mar. 1980.

[22] H. Zhen, L. Chengwei, L. Songquan, Z. Zhenghe, and L. Dongyu, "Speckle affected fringe detection based on three envelope extraction for self-mixing displacement measurement," *Opt. Commun.*, vol. 392, pp. 100–108, Jun. 2017.

[23] S. Donati and G. Giuliani, "Analysis of the signal amplitude regimes in injection detection using laser diodes," in *Proc. Phys. Simul. Optoelectron. Devices VIII*, Jul. 2000, pp. 639–644.

[24] C. Kim, C. Lee, and O. Kwonhyok, "Effect of linewidth enhancement factor on fringe in a self-mixing signal and improved estimation of feedback factor in laser diode," *IEEE Access*, vol. 7, pp. 28886–28893, Mar. 2019.

[25] Z. Huang, "Piece-wise transition detection algorithm for a self-mixing displacement sensor," *Chin. Opt. Lett.*, vol. 11, no. 9, pp. 8–12, Sep. 2013.

[26] R. Kliese, T. Taimre, A. A. A. Bakar, Y. L. Lim, K. Bertling, M. Nikolić, J. Perchoux, T. Bosch, and A. D. Rakić, "Solving self-mixing equations for arbitrary feedback levels: A concise algorithm," *Appl. Opt.*, vol. 53, no. 17, pp. 3723–3736, Jun. 2014.

[27] L. G. Dunfield and J. F. Read, "Determination of reaction rates by the use of cubic spline interpolation," *J. Chem. Phys.*, vol. 57, no. 5, pp. 2178–2183, Sep. 1972.

[28] A. Dandridge, A. Tveten, and T. Giallorenzi, "Homodyne demodulation scheme for fiber optic sensors using phase generated carrier," *IEEE J. Quantum Electron.*, vol. 18, no. 10, pp. 1647–1653, Oct. 1982.

[29] J. He, L. Wang, F. Li, and Y. Liu, "An ameliorated phase generated carrier demodulation algorithm with low harmonic distortion and high stability," *J. Lightw. Technol.*, vol. 28, no. 22, pp. 3258–3265, Nov. 15, 2010.

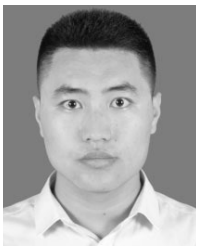

ZIHUA ZHANG received the B.E. degree in electronic science and technology and the M.S. degree in mechanical and electronic engineering from Northeast Petroleum University, China, in 2012 and 2015, respectively. He is currently pursuing the Ph.D. degree with the School of Instrumentation Science and Engineering, Harbin Institute of Technology, China.

His research interests include optical feedback in lasers for industrial applications, data acquisition, and signal processing.

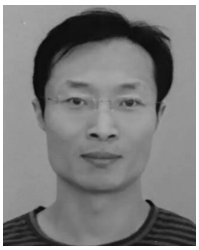

CHUNLEI JIANG received the Ph.D. degree from the School of Instrumentation Science and Engineering, Harbin Institute of Technology, Harbin, China, in 2017. From November 2018 to November 2019, he studied with Bangor University, U.K., as a Visiting Scholar.

He is currently a Professor with the College of Electrical and Information Engineering, Northeast Petroleum University, China. His research interests include precision measurement, self-mixing interference, and ultraprecision detection.

LIQUN SHEN received the B.E. degree in electrical engineering and automation, the M.S. degree in control theory and control engineering, and the Ph.D. degree in control science and engineering from the Harbin Institute of Technology, Harbin, China, in 2002, 2004, and 2008, respectively. From November 2012 to November 2013, he studied with the School of Electrical and Information Engineering, The University of Sydney, as a Postdoctoral Fellow.

He is currently a Vice Professor with the Department of Instrumentation Science and Technology, Harbin Institute of Technology. His research interests include laser photoelectric detection technology and MATLAB simulation modeling.

CHENGWEI LI received the B.E. and M.S. degrees in measurement technology and instruments and the Ph.D. degree in precision instruments and machinery from the Harbin Institute of Technology, Harbin, China, in 1985, 1988, and 2000, respectively. From 1997 to 1998, he studied with the Department of Computer Science, University of Hamburg, Germany.

He is currently a Professor with the Department of Instrumentation Science and Technology, Harbin Institute of Technology. His research interests include laser photoelectric detection and ultraprecision detection technology.

ZHEN HUANG received the B.E. degree in electronic science and technology from Fujian Normal University, China, in 2004, the M.S. degree in instrumentation science and technology from Yanshan University, China, in 2007, and the Ph.D. degree in instrumentation science and technology from the Harbin Institute of Technology, Harbin, China, in 2014.

She is currently a Vice Professor with the School of Physics Science and Technology, Lingnan Normal University, Zhanjiang, China. Her research interests include laser optical feedback, diode-laser sensors, and sensing systems.